Recombination rate saturation mechanisms at oxidized surfaces of high-efficiency silicon solar cells

S. J. Robinson, S. R. Wenham, P. P. Altermatt, A. G. Aberle,[a] G. Heiser,[b] and M. A. Green[c]
Centre for Photovoltaic Devices and Systems, University of New South Wales, Sydney 2052, Australia

(Received 3 April 1995; accepted for publication 19 May 1995)

Shoulders have been observed in the measured semilogarithmic current-voltage ($I-V$) characteristics of high-efficiency passivated emitter and rear locally diffused silicon (Si) solar cells. An improved understanding is given of the mechanism proposed to cause these nonideal $I-V$ curves. It is shown that this mechanism is due to the electrostatic behavior of free carriers at the Si/SiO_2 interface of oxidized Si devices in which the Si adjacent to the oxide is depleted (or in some cases, inverted) at equilibrium, and results in saturation of the surface recombination rate. Two-dimensional numerical computer simulations are used to investigate this mechanism and its effect on cell performance. In addition, the simulations provide a means of estimating the extent to which lateral conduction in the rear surface channel also contributes to the observed recombination saturation in these cells. It is shown that ohmic limitation of lateral conduction occurs, however, the lateral current flows are negligible in comparison to the recombination currents due to the former mechanism.

I. INTRODUCTION

Recent measurements of high-efficiency passivated emitter and rear locally diffused (PERL)[1] and passivated emitter and rear floating-junction (PERF)[2] silicon solar cells fabricated at the University of New South Wales (UNSW) have exhibited similar shoulders in the intermediate-bias regions of the semilogarithmic dark $I-V$ characteristics. The "tops" (or high-current sections) of these shoulders are also observed in the semilogarithmic illuminated $I-V$ characteristics (after the curve has been shifted by the short-circuit current J_{sc}).[3] Two very different causes have been proposed for these nonideal characteristics: The behavior of PERL cells has been attributed[4–7] to the combination of

(i) interface states exhibiting unequal electron and hole capture cross sections,
(ii) band bending due to fixed positive charge in the oxide and Al/p-Si work-function difference, and
(iii) the quasicontinuum of Si/SiO_2 interface states with energy-dependent capture cross sections.

In contrast, the behavior of PERF cells (which are identical to PERL cells except that they have an n-diffused layer across the rear surface, but masked from the point contacts) has been attributed to an ohmic limitation of the lateral current flowing through the uncontacted rear diffused layer toward regions of high recombination.[2] In this study we concentrate on the PERL cells, and only briefly consider PERF cells.

Many theories have been proposed to describe recombination at oxidized Si surfaces. The early work of Frankl[8] made many approximations which severely restricted its applicability. Grove and Fitzgerald[9] and later Hurkx *et al.*[10] considered the particular situation that occurs when a p-n junction depletion region reaches the surface space-charge region. Rees[11] and De Visschere[12] considered the case where the surface band bending is purely a result of trapped charge in discrete acceptorlike states, as well as making some limiting assumptions which restricted their theories to surfaces depleted at equilibrium. A number of authors[13–15] took the surface potential as an independent parameter which can be controlled externally. In practice it is nearly impossible to maintain a fixed surface potential at high injection levels, even using a gate voltage, due to the interdependence of the surface potential and the carrier concentrations (see Secs. IV and V); however, the most general of these approaches (that of Dhariwal and Mehrotra[14]) gives an idea of the importance of diffusion through the surface space-charge region, relative to recombination at the interface itself.

The theories of Girisch, Mertens, and De Keersmaecker,[16] Correig *et al.*,[17] Aberle, Glunz, and Warta,[18] and Otaredian[19] come closest to explaining the experimentally observed "saturation" behavior of PERL cells. Girisch and co-workers were principally concerned with the dependence on gate voltage, while the others all concentrate on the effective surface recombination velocity (see Sec. V for definition). Correig *et al.* and Otaredian give purely theoretical treatments of the problem. Correig *et al.* do consider recombination currents, and mention a scenario where a constant recombination rate is predicted. They attribute this behavior to diffusion through the p-n junction (close to the surface); however, implicit in their argument is a very high interface recombination current which is not relevant to high-efficiency devices. The theoretical framework given by Otaredian is the most general (although only bare oxides are considered), but the approximate solutions given (and their interpretations) cannot be applied here.

In this work we extend the theories of Girisch and co-workers, Correig *et al.*, Aberle and co-workers, and Otare-

[a]On leave from: Institut für Solarenergieforschung, D-31860 Emmerthal, Germany.
[b]Also with: School of Computer Science and Engineering, University of NSW, Australia.
[c]Electronic mail: m.green@unsw.edu.au

 0021-8979/95/78(7)/4740/15/$6.00

dian to include the physical situation apparent in PERL and PERF cells. In particular, we extend the model for band bending at the oxidized surfaces [(ii) above] to include the effect of a nonuniform dopant profile in the Si, and concentrate on the behavior of the surface carrier concentrations as the bulk injection level is varied. This has lead to a significantly improved understanding of the precise mechanism of recombination at oxidized surfaces of silicon devices. For example, it is shown that recombination saturation at oxidized surfaces can be caused by band bending alone (with equal electron and hole capture cross sections).

As will become evident, the electrostatic conditions at the Si/SiO_2 interface are critical to the understanding of surface recombination rates in PERL cells. Hence, in Sec. II we present an overview of these conditions, followed (in Sec. III) by the measured parameters of the oxides used in PERL cells. The measured oxide parameters provide a starting point for the calculations presented in Sec. IV of the carrier concentration profiles in the Si as a function of bulk injection level. Here we give both an approximate analytical solution and the results of more general numerical simulations (the only approximations in the latter being the use of a single interface state and an invariant trapped charge density). In Sec. V the details of the mechanism of saturation caused by the electrostatic conditions at an oxide-covered Si surface are presented. In that section we also investigate the extent to which the "lateral conduction effect" is evident in the PERL cell structure, and similarly the degree to which the "electrostatic effect" is important in PERF cells. Finally, in Sec. VI we discuss the expected shape of the $I-V$ characteristics resulting from the saturation behavior and compare this to measured data from PERL cells (which exhibit independently confirmed 1 sun efficiencies above 23%).

II. ELECTROSTATICS AT Si/SiO_2 INTERFACES

Oxide-passivated surfaces of p-n junction silicon solar cells fall into two basic categories: bare oxides (frequently used at the front surface) or those covered by a metal (employed at the rear surface of most high-efficiency devices). These two cases exhibit notably different electrostatic characteristics, although in the limit of very thick oxides their characteristics converge, as becomes evident below. Both surface structures have been shown to influence the performance of high-efficiency Si solar cells.[20] However, since the effect of the electrostatic conditions on recombination at bare oxides is relatively well understood,[19] we treat the metal-oxide-silicon (MOS) system in detail here, and only briefly compare the two systems.

A schematic diagram of the MOS system showing its charge distribution and band structure is given in Fig. 1 (the bulk silicon is taken to be p type but the n-type case is analogous). Our modeled system allows for fixed oxide charge, interface trapped charge, a metal-semiconductor work-function difference, a gate voltage, and a nonuniform semiconductor dopant distribution. In many MOS applications the system is never taken far away from equilibrium conditions; however, when employed to provide surface passivation in solar cells, the injection level in the bulk silicon depends on the illumination level and bias voltage across the

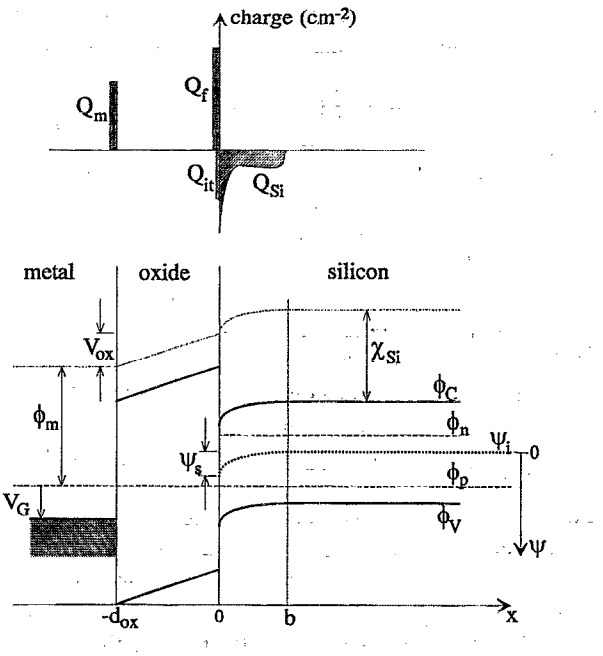

FIG. 1. Charge distribution and band diagram for a metal/SiO_2/(p-type)Si system under nonequilibrium conditions. The x direction is perpendicular to the plane of the Si/SiO_2 interface. Charge densities are measured in elementary charges per cm^2.

whole device. Consequently, we also allow for unequal electron and hole quasi-Fermi levels. As can be seen in Fig. 1, a one-dimensional approximation of the MOS system has been adopted. The geometry of the MOS structures found in solar cells is usually essentially planar (for example, at the rear surface of PERL cells), justifying a one-dimensional approach in such cases.

The model used for the interface trapped charge is outlined in the Appendix. The quantum-mechanical trapping of charge at interface states is commonly modeled using several (lumped) parameters which are, in principle, measurable; however, many of these parameters have not yet been successfully measured (for any oxides), making a quantitative analysis impossible. Furthermore, the measured fixed oxide charge contains a contribution from interface trapped charge (and also from distributed oxide charge). Thus, we give a qualitative discussion of the effects of interface trapped charge rather than attempting to include the statistics directly into our calculations. We also assume that the oxide thickness is sufficiently large (i.e., greater than ~50 Å) to render tunneling currents negligible, and that the oxide contains no mobile charge. Apart from these relatively minor restrictions, this model represents the general case of a MOS system.

In Fig. 1 Q_f is the density of fixed oxide charges. These have been experimentally determined to lie adjacent to the Si, in a layer thin enough to be well approximated by a sheet charge at the Si/SiO_2 interface.[21] There is also some fixed charge distributed through the oxide in real devices, but its effect can be modeled as a contribution to Q_f, and the measured value of Q_f includes this contribution. Q_{Si} is the total charge density induced in the Si, consisting of ionized dopants in the space-charge region and free carriers in any inversion or accumulation layer. Q_m is the density of charges at

the metal/SiO_2 interface, and Q_{it} the charge density trapped in the interface states (see the Appendix). All charges are measured in "elementary charges" per cm^2. ψ is the electrostatic potential (measured relative to the intrinsic Fermi potential $\psi_i=-E_i/q$ in the quasineutral bulk), ψ_s is the so-called "surface potential" at the Si/SiO_2 interface, V_G the applied gate (i.e., metal-bulk Si) voltage, and V_{ox} is the potential drop across the oxide. ϕ_m is the metal work function, χ_{Si} (=4.05 V)[22] the silicon electron affinity, and ϕ_C ($=-E_C/q$) and ϕ_V ($=-E_V/q$) are the conduction- and valence-band-edge potentials, respectively. The oxide thickness is d_{ox} and the plane at which band bending ceases is $x=b$. The electron and hole quasi-Fermi levels $\phi_n(x)$ and $\phi_p(x)$ are defined in the standard way by[22]

$$n=n_i e^{q(\psi-\phi_n)/kT}, \quad p=n_i e^{q(\phi_p-\psi)/kT}, \tag{1}$$

where n_i is the intrinsic carrier concentration, q the electronic charge, k Boltzmann's constant, and T the absolute temperature. We further label the separation of the quasi-Fermi levels as $V(x)$. Under low-injection conditions and for long diffusion lengths in the bulk regions, the quasi-Fermi-level separation at the edge of the surface space-charge region $V(b)$ is approximately equal to the voltage across the whole device (and can be a result of illumination and/or an applied bias voltage).

The carrier concentrations at the Si/SiO_2 interface can be deduced from Eq. (1),

$$n_s=n_i e^{q[\psi_s-\phi_n(x=0)]/kT},$$
$$p_s=n_i e^{q[\phi_p(x=0)-\psi_s]/kT}. \tag{2}$$

Hence, the determination of the carrier densities is reduced to the calculation of the quasi-Fermi levels and the surface potential ψ_s. In order to determine ψ_s for p-type Si one must solve the following equations (the equations for n-type are identical provided ϕ_p and $n_i^2/N_{A,b}$ are replaced by ϕ_n and $N_{D,b}$, respectively):[23]

$$V_G=\phi_m+V_{ox}+\psi_s-\chi_{Si}-(\phi_p-\phi_C)|_{x=b}, \tag{3}$$

where

$$(\phi_p-\phi_C)|_{x=b}=\frac{kT}{q}\ln\left(\frac{N_C N_{A,b}}{n_i^2}\right), \tag{4}$$

$$V_{ox}=\int_{-d_{ox}}^{0}\xi_{ox}\,dx, \tag{5}$$

$$\epsilon_{Si}\xi_{Si}|_{x=0}-\epsilon_{ox}\xi_{ox}|_{x=0}=\rho_s=q(Q_f+Q_{it}), \tag{6}$$

and

$$\frac{\partial\xi_{Si}}{\partial x}=\frac{\rho_{Si}}{\epsilon_{Si}}\approx\frac{q}{\epsilon_{Si}}[p(x)-n(x)-N_A(x)+N_D(x)]. \tag{7}$$

Equation (3) results from the fact that the total change in the majority-carrier quasi-Fermi level across the MOS system must equal the applied gate voltage. Note that the condition of total charge neutrality over the system (i.e., $Q_f+Q_{if}+Q_{Si}+Q_m=0$) can be used instead of Eq. (3)[16,18] to give identical results. In Eq. (4), N_C is the effective density of states in the conduction band, and N_A the ionized acceptor dopant density with the subscript b referring to the bulk quasineutral silicon (i.e., $x\geq b$). Equation (5) expresses the relationship between the potential and electric field ξ_{ox} in the oxide, while Eq. (6) is Gauss's law applied to the SiO_2/Si interface (where ϵ_{Si} and ϵ_{ox} are the silicon and oxide permittivities, ξ_{Si} is the electric field in the silicon, and ρ_s is the interface charge density), and Eq. (7) is the one-dimensional form of Poisson's equation. Equation (7) has been solved for $\xi_{Si}|_{x=0}$ in the general case (assuming only constant quasi-Fermi levels).[23] Since $x=b$ is defined to be the plane where band bending ceases, $\xi_{Si}|_{x\geq b}=0$, and

$$\xi_{Si}|_{x=0}=\left(\frac{2kT}{\epsilon_{Si}}[(n_s-n_b)+(p_s-p_b)]+\frac{2q}{\epsilon_{Si}}\int_{\psi_b}^{\psi_s}N_A\,d\psi\right)^{1/2}. \tag{8}$$

Also, in the quasineutral p-type bulk,

$$p_b=N_{A,b}+\Delta n_b, \tag{9}$$

where $\Delta n_b=(n_b-n_{0,b})$, and $n_{0,b}$ is the equilibrium electron concentration.

The quasi-Fermi levels can be found[19] by solving the current-density and continuity equations,

$$J_n=q\mu_n n\xi+qD_n\nabla n; \tag{10}$$

$$J_p=q\mu_p p\xi-qD_p\nabla p, \tag{11}$$

$$\nabla J_n=q(U-G), \tag{12}$$

$$\nabla J_p=-q(U-G), \tag{13}$$

where μ_n and μ_p are the electron and hole mobilities, D_n and D_p the diffusivities, and $U(x)$ and $G(x)$ are the recombination and generation rates, respectively.

Equation (3) can also be applied to the case of a bare oxide; however, due to the difficulty in defining a Fermi potential in an insulator (particularly under nonequilibrium conditions), the mathematical formulation of the bare-oxide electrostatics is usually approached from a different perspective. In this case Eqs. (6) and (7) can be solved directly. Further, if one assumes constant quasi-Fermi potentials in the Si, then Eq. (7) again reduces to Eq. (8). In general there will be some two- or three-dimensional effects arising from metal contacts (such as the front grid), voltage drops along diffused layers (such as the emitter), distributed oxide charge, and charge attracted from the surroundings to the outer SiO_2 interface. These all result in a nonzero value for the electric field in the oxide ξ_{ox}. However, in most practical cases the oxide thickness is large enough that (for oxide regions well separated from the metal contacts) ξ_{ox} is negligibly small in comparison to ξ_{Si} close to the Si/SiO_2 interface (since the fixed oxide charge is located at this interface). Hence, Eq. (6) can often be significantly simplified by assuming $\xi_{ox}\sim 0$. Comparing the bare oxide to the MOS system, one then finds that since the metal is absent, the fixed oxide charge (and interface trapped charge) cannot be partially balanced by charge in the metal, and of course there is no effect from a difference in metal and Si work functions. The band bending caused by a given fixed oxide charge Q_f (for zero work-function difference) is greater in the Si under a bare oxide

TABLE I. Measured rear-oxide parameters of n^+p PERL silicon solar cells.

	Rear oxide (on p-type Si)
Thickness d_{ox} (nm)	500–700
Covering metal work function ϕ_m (V)	4.1 (aluminium)
Fixed charge density Q_f (cm^{-2})	$(6\pm1)\times10^{10}$ (positive)[a]
Interface-state density D_{it} ($cm^{-2}\,eV^{-1}$)	$3-4\times10^9$ at midgap[b,c]

[a]Reference 25.
[b]Reference 27.
[c]Rising to larger values toward each band edge (creating a U-shaped distribution).

than it is when the oxide is covered by a metal; however, the larger the oxide thickness, the smaller is this effect. The degree of band bending caused purely by the work-function difference decreases with increasing oxide thickness, so in the limit $d_{ox}\rightarrow\infty$ one finds $\xi_{ox}\rightarrow0$, and the MOS characteristics approach those of the bare oxide system.

III. MEASURED OXIDE PARAMETERS

The measured parameters of the rear surface oxides of PERL cells are listed in Table I. The fabrication process for PERL oxides is very similar to that used for PERF cells (and many other semiconductor devices). The oxide thicknesses were measured using ellipsometry.[24] Aluminium (Al) is the only metal used at the rear surfaces of these cells. MOS capacitors fabricated using the PERL processing sequence have been analysed using capacitance-voltage ($C-V$) and small-pulse deep-level transient spectroscopy (DLTS) techniques.[18,25] These measurements provided the values for the fixed oxide charge density of Q_f and midgap interface-state density D_{it} shown in the table. The interface-state distribution (with respect to energy) was also measured and found to be a "U shape," similar to distributions previously observed.[18,26] As mentioned above, the measured value of Q_f includes some interface trapped charge (since this trapped charge does not change with injection level during the $C-V$ measurements as discussed in the Appendix) and a contribution from distributed oxide charge.

The dopant profiles in the p-type Si adjacent to the rear oxide as measured by $C-V$,[27] spreading resistance (SPR), and secondary-ion-mass spectroscopy (SIMS)[28] are shown in Fig. 2(a). The $C-V$ measurements were taken on the MOS capacitors mentioned above, while the SPR and SIMS data were obtained from unmetallized oxidized Si samples. It is well known that, due to the difference in equilibrium concentrations of dopants in Si and SiO_2, there is a redistribution of dopants during thermal oxidation.[29,30] The exact form of the redistribution depends on the oxidation conditions (such as temperature, atmosphere, and oxidation and annealing times) and the physical properties of the silicon (such as the segregation coefficient and dopant diffusivity).[30,31] The UNSW oxides are grown under a dry oxygen atmosphere containing 2% of trichloroacetylene (TCA). A simulation of this type of oxidation was performed using the program SUPREM,[32] but assuming a pure dry oxygen atmosphere (since SUPREM does not allow for TCA). The results of this simulation in Fig. 2(a) show that the measured profiles are consistent with the accepted theory of dopant redistribution. It should be noted that the SPR data are unreliable within 0.05 μm of the interface[33,34] and the $C-V$ data are limited to distances from the interface greater than about two extrinsic Debye lengths[35,36] (i.e., greater than about 0.1 μm in this case). The elemental sensitivity of the SIMS measurements to boron and phosphorus is high (better than 1 part per billion or 10^{13} cm^{-3} in Si);[28,37] however, this only applies to relative magnitudes, so the SIMS results are always referenced to a known dopant concentration (in this case that of the uniformly doped bulk region).

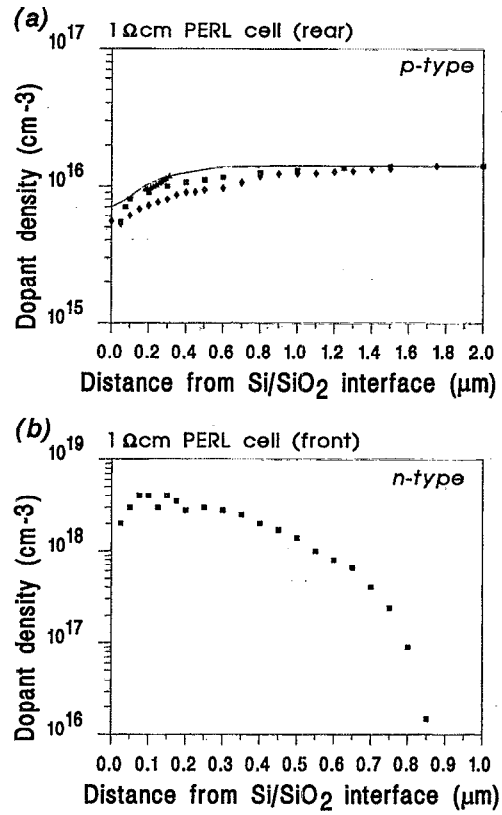

FIG. 2. Measured and simulated dopant profiles near the surface of thermally oxidized (a) p-type silicon, and (b) n-diffused silicon. The triangles, squares, and diamonds were obtained from capacitance-voltage, spreading resistance, and secondary-ion-mass spectroscopy measurements, respectively. The line in (a) shows the profile calculated from simulations.

In Fig. 2(b) the dopant profile in the n-diffused emitter surface region, as measured by SPR, is shown. No attempt was made to simulate dopant redistribution in this case due to uncertainty in the form of the dopant distribution prior to oxidation.

Neither Q_f or D_{it} have been measured on PERL (or PERF) cell n-diffused oxidized surfaces, although they have been measured on uniformly doped n-type wafers oxidized using the PERL processing sequence.[25] The fixed oxide charge for uniformly doped 1 Ω cm wafers of this type is about 8×10^{10} cm^{-2} (positive) and D_{it} is about 5×10^9 $cm^{-2}\,eV^{-1}$ at midgap.[25] Both D_{it} and Q_f for n-diffused oxides could differ markedly from these values due to the properties of the diffusion process and the higher surface dopant concentration;[38] however, for these high n-type dopant den-

sities, it is found that the results of the simulations are essentially independent of the magnitude of Q_f (see Sec. IV B). Also, the measured values[25] suggest that fixed oxide charge at the Si/SiO_2 interface is only weakly dependent on doping level and type. Only the product of D_{it} and the electron or hole "capture cross section" (see Sec. V for definition of these parameters) needs to be specified in the simulations; hence, no attempt was made to assign an explicit value to D_{it} at the n-diffused oxidized surfaces of either the PERL or PERF cells. The front oxides of these cells are bare except for a small coverage of titanium, palladium, and silver of the front grid.

Measurements of electron and hole capture cross sections σ_n and σ_p (see Sec. V) for interface states at oxidized Si surfaces vary over a wide range in the literature. A comprehensive summary of past values can be found in the work of Aberle and co-workers,[18] with most values falling in the ranges of 10^{-16}–10^{-14} cm^2 for σ_p and 10^{-17}–10^{-12} cm^2 for σ_n. The DLTS measurements on UNSW MOS structures mentioned above have also been used to determine capture cross sections.[25] Near-midgap values of $\sigma_p \sim 2\times10^{-16}$ cm^2 and $\sigma_n \sim 10^{-14}$ cm^2 were obtained, which are in good agreement with the previous measurements. Together, these data suggests that the ratio of electron and hole capture cross sections for midgap defect levels is $\sigma_p/\sigma_n \sim 0.01$. Except for some data obtained on bulk energy levels caused by specific elemental impurities,[39] and recent measurements using a modified version of DLTS,[40] only either the electron or the hole capture cross section for a particular defect has in general been reported. Indeed, for interface states (as distinct from bulk defects) small-pulse DLTS, which is only capable of measuring majority-carrier capture cross sections, has been the most widely used technique. In these measurements, p-type wafers are used to determine σ_p and n-type wafers to determine σ_n. Hence, it is possible that the midgap cross sections reported in Refs. 18 and 25 actually refer to different types of interface state (both located at midgap), in which case no σ_p/σ_n ratio for a particular type of midgap state can be inferred from these measurements.

Measurements by Yablonovitch *et al.*[41] suggest that for $n_s/p_s < 0.1$, the ratio σ_p/σ_n for the defect levels which dominate surface recombination is of the order of 0.01, as for the midgap states mentioned above (if one assumes the DLTS measurements of σ_n and σ_p do apply to the same interface state at midgap); however, the same measurements imply that for $n_s/p_s > 80$, the ratio σ_p/σ_n for the defect levels which dominate surface recombination can be of the order of 80. For $0.1 < n_s/p_s < 80$, the measurements suggest $\sigma_p/\sigma_n \sim 1$ for the dominant states. Independent photoluminescence measurements by Stein and Röppischer[42] also suggest that $\sigma_p/\sigma_n > 1$ for large n_s/p_s. Yablonovitch *et al.*'s measurement technique does not determine the energy level of the dominant states, although, as is discussed in Sec. V, states near midgap are likely to dominate the recombination rate. This suggests that either defect levels at midgap are not always those via which the recombination primarily takes place, or there is more than one type of interface state at midgap. In the latter case, either the measurement techniques quoted in Refs. 18 and 25 only detected one type of state (due to the particular n_s/p_s ratio used—which, at least in Ref. 25, is much less than unity[43]), or the reported midgap cross sections refer to different states (as mentioned above). There is further experimental evidence for chemically different interface states producing allowed levels at the same energy within the band gap in the work of Uren, Brunson, and Hodge.[44] Indeed, it is possible that the dependence of the charge associated with the interface state on its occupancy (for example, whether it is donor- or acceptorlike, or able to accept more than one carrier), can result in different σ_p/σ_n ratios. Yablonovitch *et al.*'s measurements were made on MOS devices with oxides grown in a similar fashion to those fabricated at UNSW, and appear to be the only data taken as a function of n_s/p_s.

IV. SURFACE CARRIER CONCENTRATIONS AS A FUNCTION OF BULK INJECTION LEVEL

As becomes evident below, a good understanding of the dependence of the surface carrier concentrations on the bulk injection level is critical to the analysis of recombination saturation in PERL cells. Hence, we examine this dependence in detail before considering the net effect on the recombination rate.

The equations introduced in Sec. II can be solved analytically in a few special cases which give considerable insight into the electrostatics of the general case. For the analytical calculations below, we assume constant quasi-Fermi levels across the surface space-charge region. This is a good approximation for low surface recombination rates, high bulk lifetimes, and a spatially uniform generation rate in the surface region (all of which are applicable to PERL cell rear surfaces). If the dopant concentration in the (p-type) Si is uniform, low-injection and depletion conditions hold in the bulk and surface regions, respectively (i.e., $n_b, n_s, p_s \ll N_A$), and, provided Q_{it} is not strongly voltage dependent (see the Appendix), then

$$\psi_s = \frac{kT}{q} + \left\{ \left[\frac{d_{ox}^2 q N_A \epsilon_{Si}}{2\epsilon_{ox}^2} - \left(V_\Delta - \frac{d_{ox} q (Q_f + Q_{it})}{\epsilon_{ox}} + \frac{kT}{q} \right) \right]^{1/2} - \frac{d_{ox}}{\epsilon_{ox}} \left(\frac{q N_A \epsilon_{Si}}{2} \right)^{1/2} \right\}^2, \tag{14}$$

where

$$V_\Delta = \phi_m - V_G - \chi_{Si} - (\phi_p - \phi_C)|_{x=b}. \tag{15}$$

Note that in this case ψ_s is essentially independent of the device voltage. The surface carrier concentrations are then given by substituting Eq. (14) into Eq. (2), with the result that p_s is independent of voltage (since $\phi_p \sim$const) while $n_s \sim \exp(qV/kT)$.

As the bulk injection level increases, the surface approaches strong inversion conditions and the equations for ψ_s become implicit, requiring numerical solution. In this work we use the semiconductor device simulation program DESSIS$_{ISE}$ (formerly SIMUL)[45] to simulate the entire PERL cell structure. In particular, the program provides a numerical solution to the electrostatic equations for the MOS and bare oxide structures found at the rear and front surfaces of PERL

TABLE II. Parameters used in the 2D simulations of the PERL cell structures.

Cell structure	n^+p rear locally contacted Si solar cell, planar and rear surface
Substrate	Uniformly doped p-Si at 1.41×10^{16} cm^{-3} (1 Ω cm) except for region near the rear Si/SiO_2 interface, where the dopant profile of Fig. 2(a) is used; 370 μm thick
Front contacts	Parallel fingers, spacing 0.8 mm, metal–Si interface 3 μm, finger shading width 20 μm
Rear contacts	Parallel fingers, spacing 0.26 mm, metal–Si interface 10 μm
n^+ diffusion	Gaussian, $N_s=5\times10^{18}$ cm^{-3}, depth=1.0 μm, ρ_s=200 Ω/□
Front local n^{++} diffusion	Gaussian, $N_s=1\times10^{20}$ cm^{-3}, depth=2.0 μm, width=6.2 μm, ρ_s=11 Ω/□
Rear local p^+ diffusion	Gaussian, $N_s=5\times10^{19}$ cm^{-3}, depth=5 μm, ρ_s=11 Ω/□ (diffusions are 20 μm wider than the rear metal contacts).
Temperature	298 K
Illumination spectrum	AM1.5 Global (100 mW/cm^2)
Contact resistance	10^{-6} Ω cm^2
Band-gap narrowing model	Bennett–Wilson[a] (BW)
Perimeter recombination	1 sun V_{oc} is adjusted to be 6 mV higher than that measured (see Ref. 20)
SRH bulk recombination	Midgap traps with $\sigma_n=\sigma_p$, effective low-level injection SRH electron lifetime 1.0 ms
Radiative recombination	Neglected
Auger recombination	$C_n=1.2\times10^{-30}$ cm^6 s^{-1}, $C_p=1.2\times10^{-30}$ cm^6 s^{-1}[b]
Surface recombination model:	
(a) metal contacts	Flatband, midgap traps, $S_{n0}=S_{p0}\geqslant10^7$ cm s^{-1}
(b) front oxidized surface	Bare oxide with d_{ox}=100 nm and $Q_f=8\times10^{10}$ cm^{-2} Midgap traps, with $S_{n0}=S_{p0}$=2000 cm s^{-1}
(c) rear oxidized surface	Two cases considered, both of which are MOS structures: d_{ox} ϕ_m, Q_f, D_{it} as given in Table I for both cases (i) Midgap traps, $S_{n0}=S_{p0}$=20 cm s^{-1} ($\sigma_n=\sigma_p=5.7\times10^{-16}$ cm^2) (ii) Midgap traps, S_{n0}=1000 cm s^{-1} ($\sigma_n=2.9\times10^{-14}$ cm^2), S_{p0}=10 cm s^{-1} ($\sigma_p=2.9\times10^{-16}$ cm^2)
Mobility	Doping-dependent model of Masetti and co-workers[c]
Intrinsic carrier-density model	Modified BW with n_i (300 K)=1.00×10^{10} cm^{-3} of Sproul and Green[d]

[a]H. S. Bennett and C. L. Wilson, J. Appl. Phys. **55**, 3582 (1984).
[b]R. A. Sinton and R. M. Swanson, IEEE Trans. Electron Devices **ED-34**, 1380 (1987).
[c]G. Masetti, M. Severi, and S. Solmi, IEEE Trans. Electron Devices **ED-30**, 764 (1983).
[d]A. B. Sproul and M. A. Green, J. Appl. Phys. **70**, 846 (1991).

cells. The parameters used in the simulations are given in Table II. Most important, the front and rear surface regions are modeled as outlined in Sec. II and Fig. 1. Since, for technological reasons,[18] a gate voltage cannot presently be successfully applied to the PERL structure, we only consider the case $V_G=0$ here. Also, we neglect the electrostatic effect of the front metal grid since its coverage over oxide is very small. Two-dimensional (2D) simulations were performed, providing a good approximation to the real device operation, without requiring the long computing times of 3D simulations. Note that in these numerical calculations no constancy of the quasi-Fermi levels is assumed, so that the effects of recombination, generation, diffusion, and drift of carriers within the surface space-charge region are properly included. The 2D model thus includes both the full electrostatics of the rear oxide (except for the region within about an oxide thickness of the point metal contacts) and the possible effects of lateral conduction within a surface inversion layer towards regions of high recombination (such as the rear contacts or pinholes in the oxide).

A. Rear surface

Figure 3 shows the calculated carrier concentrations in the rear surface region (away from the contacts) of a typical 1 Ω cm PERL cell, under four particular bulk injection levels. The injection levels were chosen to correspond to specific conditions at the Si SiO_2 interface. In condition A, the surface region is depleted (at equilibrium) with $n_s/p_s<1$. Condition B occurs when $n_s/p_s=1$ (and is therefore the point beyond which the surface is inverted), while for condition C, n_s has increased to the point where it is no longer negligible with respect to the surface dopant concentration $N_{A,s}$. As the bulk injection level is increased beyond C, the surface goes into "strong" inversion (when $n_s\sim N_{A,s}$). Finally, the bulk becomes highly injected (with the surface still strongly inverted), and this is condition D.

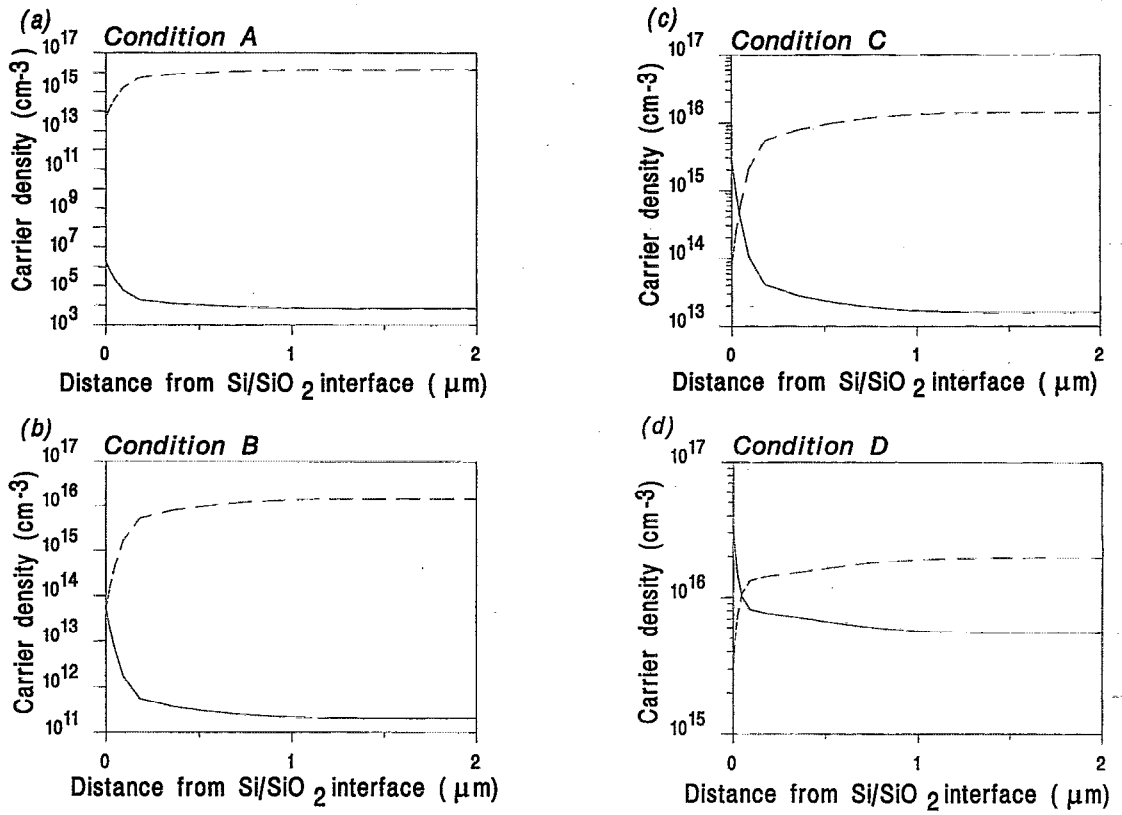

FIG. 3. Calculated electron (solid lines) and hole (dashed lines) carrier concentrations near the rear Si/SiO_2 interface of a 1 Ω cm n^+p PERL Si solar cell, under particular bulk injection levels. The bulk injection increases from equilibrium conditions in (a) to high injection conditions in (d). The cell parameters are given in Table II.

The dependence on device voltage of the surface and bulk ($x \geqslant b$) carrier concentrations at the rear of 1 Ω cm PERL cells, both in the dark and under 1 sun illumination, is shown in Fig. 4. Consider first the dark case [Fig. 4(a)]. As shown above analytically for a uniform dopant profile, the surface hole concentration does not increase significantly with bulk injection level until the surface electron concentration approaches the surface dopant concentration (i.e., until strong inversion is approached); however, n_s becomes greater than p_s at a lower bulk injection level, and well before bulk high injection conditions. When the surface is in strong inversion and while the bulk has not yet reached high injection, n_s increases much slower with V than n_b or p_s (p_s increases faster with V than n_s since ψ_s reduces with V). Note that the surface only goes into high injection in the sense of $n_s \sim p_s$ for very high bulk injection levels (above 0.8 V in this case).

Under 1 sun illumination [Fig. 4(b)], photogeneration results in the rear surface being inverted at short circuit. Consequently, condition B has already been "passed" and the Si/SiO_2 interface is nearly at condition C, although at a particular reduced light intensity condition B would be observed at short circuit. Furthermore, under 1 sun illumination the ratio n_s/p_s is relatively invariant (ranging between 10 and 50), in contrast to the dark case where n_s/p_s varies between about 5×10^{-8} and 50. This has implications for the curve fitting in Sec. VI.

Note that for Figs. 3 and 4, $Q_f=6.5\times10^{10}$ cm^{-2}, $d_{ox}=600$ nm, $S_{p0}=20$ cm s^{-1}, $S_{n0}=20$ cm s^{-1}, $\phi_n=4.1$ eV, and the dopant profile is as shown in Fig. 2 (i.e., the surface boron concentration depleted relative to the bulk by a factor of 2.4). For increased oxide charge, decreased oxide thickness, increased boron depletion, and/or decreased metal work function, the band bending increases, the equilibrium hole concentration (p_{s0}) decreases, and the equilibrium electron concentration (n_{s0}) increases. In such cases the medium-high voltage region of Fig. 4(a) gets stretched out and shifted down in voltage. Changing the ratio of S_{n0} and S_{p0} (or, equivalently, the capture cross sections) can have an effect on the voltage dependence of the carrier concentrations. If there is a large degree of band bending or if $\sigma_p/\sigma_n<1$ then one observes a region where n_s and n_b increase very quickly with voltage [i.e., $(n_s, n_b) \sim \exp(qV/AkT)$ with $A<1$]. This occurs when the recombination rate saturates (as is shown below), and is due to the change from electron- to hole-limited recombination and the subsequent "pileup" of electrons at the interface. Changing the magnitudes of S_{n0} and S_{p0} does not have an observable effect on the voltage dependence of the carrier concentrations, provided the magnitudes are not very large.

Figure 5 shows the voltage dependence of the surface and bulk carrier concentrations near the rear surface of 10 Ω cm PERL cells in the dark, as calculated using DESSIS$_{ISE}$. In this case the surface is already inverted at equilibrium, in

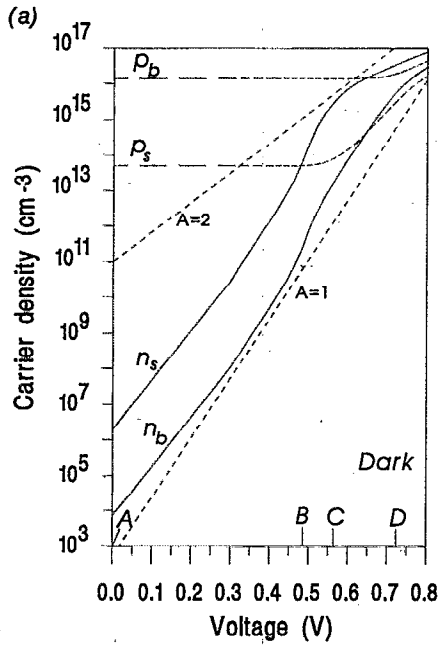

FIG. 4. Calculated voltage dependence of the electron (solid lines) and hole (dashed lines) carrier concentrations in the bulk ($x \geqslant b$) and at the Si/SiO_2 interface in the rear surface region of a 1 Ω cm n^+p PERL cell at 25 °C. The plot in (a) applies when the cell is forward biased in the dark while (b) is for a cell under 1 sun illumination. In (a) the voltages corresponding to conditions $A-D$ are indicated. Also plotted are (dotted) lines representing $(n,p)\sim\exp(qV/AkT)$, for $A=1$ and 2. The cell parameters are given in Table II.

contrast to the lower (1–2 Ω cm) base resistivity cells, so conditions A, B, and C are missing. This is also consistent with measurements taken on MOS field-effect-transistor (MOSFET) structures fabricated on substrates with various resistivities using an identical processing sequence to that for the actual PERL cells. For the 10 Ω cm cells the contrast between the rates of increase of n_s and p_s with device voltage after strong surface inversion is much clearer than for the 1 Ω cm cells.

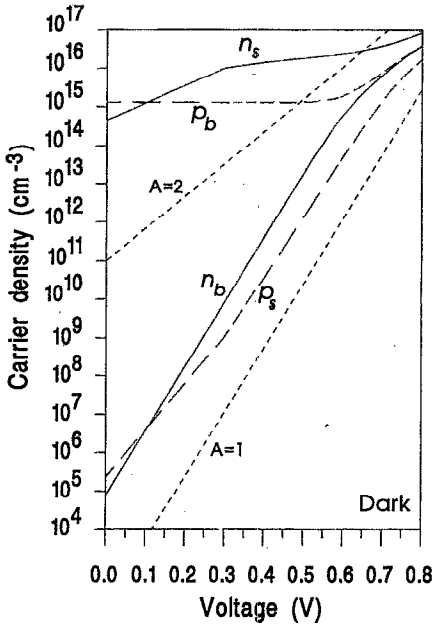

FIG. 5. Calculated voltage dependence of the electron (solid lines) and hole (dashed lines) carrier concentrations in the bulk ($x \geqslant b$) and at the Si/SiO_2 interface in the rear surface region of a 10 Ω cm PERL cell at 25 °C in the dark. Also plotted are (dotted) lines representing $(n,p)\sim\exp(qV/AkT)$, for $A=1$ and 2.

B. Front surface

The peak emitter dopant concentration at the front surfaces of PERL cells is of the order of 5×10^{18} cm^{-3} (n type), as shown in Fig. 2(b). The assumed positive oxide charge (8×10^{10} cm^{-2}) thus causes slight accumulation at the front Si/SiO_2 interface. Furthermore, it was found that the degree of surface band bending remains slight for a wide range of oxide charge densities (from zero up to about 10^{12} cm^{-2}). Hence, the calculated surface electron concentration in the dark is constant over the bias voltages considered in this work (i.e., up to 800 mV), while the hole concentration increases as $p_s\sim\exp(qV/kT)$ and is always much less than n_s. Under 1 sun illumination, p_s is also constant up to intermediate bias voltages before increasing exponentially with increasing bias, but again is always much lower than n_s.

V. RECOMBINATION SATURATION BEHAVIOR

Consider the recombination occurring via interface states at the Si/SiO_2 interface of the MOS (or bare oxide) structure. The "surface" recombination rate U_s via a single state at a potential ψ_{defect} is governed by Shockley–Read–Hall statistics,[46]

$$U_s=\frac{n_s p_s-n_i^2}{[(n_s+n_1)/S_{p0}]+[(p_s+p_1)/S_{n0}]}, \tag{16}$$

where

$$n_1 = n_i e^{q(\psi_{\text{defect}} - \psi_i)/kT},$$
$$p_1 = n_i e^{-q(\psi_{\text{defect}} - \psi_i)/kT}, \tag{17}$$

and

$$S_{n0} \equiv D_{\text{it}} v_{\text{th},n} \sigma_n, \quad S_{p0} \equiv D_{\text{it}} v_{\text{th},p} \sigma_p. \tag{18}$$

In Eq. (18) σ_n and σ_p are, respectively, the electron and hole capture cross sections, with $v_{\text{th},n}$ and $v_{\text{th},p}$ their thermal velocities (both about 10^7 cm s^{-1} at 300 K). The total recombination rate is given by the integral of U_s over all interface states. However, it is instructive to consider each state separately before performing such an integration, since different interface states may dominate over different ranges of injection level, with the net result being a rather complex envelope of the contributions from each state.

When $\psi_s \neq 0$, it is common to define a virtual surface at the plane in the bulk where the band bending ceases (i.e., $x = b$ in Fig. 1), and define an "effective" surface recombination velocity by[18,47]

$$U_s = S_{\text{eff}} \Delta n_b \quad \text{(for a } p\text{-type bulk)}. \tag{19}$$

When $\psi_s = 0$ (i.e., flatband conditions), the virtual surface becomes the Si/SiO_2 interface. S_{eff} is of practical importance since it is a measurable parameter;[18,48–51] however, in order to clearly demonstrate the saturation behavior caused by the electrostatic conditions at the Si/SiO_2 interface, we first examine the behavior of Eq. (16) directly, as a function of the bulk injection level.

A. Surface depleted at equilibrium

The rear surfaces of PERL cells with base resistivities below about 5 Ω cm satisfy this condition. Here we consider the four injection levels introduced in Figs. 3 and 4, and substitute the corresponding values for n_s and p_s into Eq. (16). Note that although Figs. 3 and 4 were obtained for a 1 Ω cm PERL cell, the general case of a semiconductor surface depleted at thermal equilibrium is entirely similar.

1. Equal capture cross sections

For the present we assume midgap interface states with equal capture cross sections for electrons and holes [i.e., $n_1 = p_1 = n_i$ and $S_{n0} = S_{p0} \equiv S_0$ in Eq. (16)].

Condition A→B: For these bulk injection levels $n_s \ll p_s$ and $p_s \sim p_{s0} = \text{const}$, so the surface recombination rate is limited by the supply of electrons to the defect level within the band gap, with

$$U_s = S_0 \Delta n_s \cong S_0 n_s \tag{20}$$

and $n_s \sim \exp(qV/kT)$ (see Sec. IV). Comparing Eqs. (19) and (20), one finds $S_{\text{eff}} \approx S_0 (n_s/n_b)$.[5] Since n_s and n_b have the same functional voltage dependence at these injection levels, S_{eff} has a constant value which is increased relative to the flatband case by the ratio of the surface to bulk electron concentrations.

Condition B: When $n_s = p_s$,

$$U_s = (S_0/2)\Delta n_s \cong (S_0/2) p_{s0}. \tag{21}$$

This is the point of transition between electron- and hole-limited behavior. Note that the magnitude of p_{s0} is a function of the degree of band bending (i.e., Q_f, Q_{it}, d_{ox}, ϕ_m, and the magnitude and profile of the dopants), as discussed in Sec. IV. Aberle and co-workers[6] investigated the effect of the rear-surface Q_f on the recombination rate at the shoulder in the semilogarithmic $I-V$ curves of PERL cells, using a bare-oxide model with no dopant depletion. There it was noted that the shoulder shifts to lower currents with increasing Q_f, due to the extra depletion of holes at the interface.

Condition B→C: Now n_s becomes large compared to p_s and still $p_s \sim p_{s0} = \text{const}$, so

$$U_s \rightarrow S_0 p_s \approx S_0 p_{s0} \equiv \text{const} \tag{22}$$

as the bulk injection level increases. It is over these injection levels that the recombination rate saturates. As the bias across the device increases (increasing the bulk injection level), the recombination rate remains approximately constant (limited by the hole supply which increases only very slowly with bulk injection); however, if the degree of band bending at equilibrium is too small then U_s will not reach this limiting value before the bulk starts to go into high injection. Correig *et al.*[17] noted a similar constancy in the recombination rate for the special case where diffusion across a p-n junction located near the Si/SiO_2 interface limits the recombination; however, this does not apply to high-efficiency devices where the recombination currents are small. A transition at the surface from electron- to hole-limited recombination has been noted by King and co-workers,[51] Green *et al.*,[52] and Aberle *et al.*,[53] however, the details of the saturation behavior were not investigated. Comparing Eqs. (19) and (22), one finds $S_{\text{eff}} \approx S_0 (p_{s0}/\Delta n_b)$. Thus, S_{eff} decreases (linearly in a double-logarithmic plot) with increasing bulk injection level during saturation.

Condition C→D: In this case $n_s \gg p_s$, so $U_s = S_0 p_s$ as in Eq. (22); however, in contrast to condition B→C, p_s increases with bulk injection (see Fig. 4).

For interface-state energies close to midgap, the above injection dependence remains basically unchanged; however, since $p_{s0} \ll p_b$ due to the band bending, the term $n_1(p_1)$ can be large relative to p_{s0} for interface-state energy levels not very far above (below) midgap. The saturation behavior described above is still observed, but S_0 is reduced by the factor $K = (1 + n_1/p_{s0})$ [or $(1 + p_1/p_{s0})$], until condition C is reached when p_{s0} must be replaced by n_s in K. Note that $K \geq 1$ for all injection levels so that the recombination rate via these "nonmidgap" states is always reduced relative to that for a midgap state with the same S_0. However, as mentioned in Sec. III, the D_{it} for states near the band edges (which are thought to originate from strained Si bonds)[26] is much higher than for those at midgap (thought to be due to dangling Si or Si—O bonds),[26] although little is known about the sizes of the minority-carrier cross sections (relative to those for the majority carriers) for the nonmidgap states. Nonetheless, it is likely that recombination occurs primarily via states not too far from midgap.

2. Effect of unequal capture cross sections

The point at which the transition between electron- and hole-limited recombination via a particular defect level occurs is given by the condition $\sigma_p/\sigma_n = n_s/p_s$. Clearly, when $\sigma_p/\sigma_n < 1$ this transition is shifted to lower bulk injection

levels than for equal capture cross sections. This has the effect of increasing the range of bulk injection level (or equivalently device voltage) over which saturation of recombination via that defect level is observed. Conversely, when $\sigma_p/\sigma_n>1$ the range is decreased. Indeed, for large enough σ_p/σ_n, the saturation regime may not occur before the surface goes into strong inversion.

Again, we initially consider midgap states. Due to the unequal capture cross sections, when the recombination is electron (hole) limited, S_0 in the above equations becomes S_{n0} (S_{p0}). Otherwise, exactly the same equations as are derived for equal capture cross sections are applicable in this case. For nonmidgap states it can be shown that the S_{n0} or S_{p0} values must also be reduced by a factor $K' \geq 1$. In this case the nonunity term in the expression for K must sometimes be multiplied or divided by the ratio σ_p/σ_n, but otherwise K' has the same form as K.

From the work of Yablonovitch *et al.*[41] it can be seen that the σ_p/σ_n ratio of the states via which recombination primarily takes place may change as the n_s/p_s ratio changes (i.e., different interface states may dominate at different injection levels). In the case of the rear surface of 1 Ω cm PERL cells in the dark, n_s/p_s changes dramatically from about 5×10^{-8} to about 50 as the bulk injection level is increased [see Fig. 4(a)]. Thus, according to Yablonovitch *et al.*'s data, σ_p/σ_n for the dominant interface states would change from 0.01 to about 1 and then perhaps even reach 80, in these PERL cells, under increasing forward bias in the dark. The onset of saturation starts at the injection level applicable to $\sigma_p/\sigma_n=0.01$ under this scenario. Depending on the magnitudes of σ_p and σ_n and the number of different interface-state types which significantly contribute to the recombination rate, there may be a number (or even a continuum) of saturation levels in the recombination as the bulk injection level increases; however, the bulk injection level at which saturation ceases is independent of the σ_p/σ_n ratio (since it is determined purely by when the surface hole concentration starts to increase). Interestingly, as mentioned in Sec. IV for 1 Ω cm PERL cells under 1 sun illumination, $n_s/p_s\sim10$–50 for all bias voltages [Fig. 4(b)], so one would expect σ_p/σ_n for the dominant states to be nearly constant at about unity (or possibly as large as 80).

B. Surfaces inverted or accumulated at equilibrium

If the Si at the Si/SiO_2 interface is inverted or accumulated under thermal equilibrium conditions then there is no crossover of the magnitudes of n_s and p_s as the bulk injection level is increased; however, for the inverted case (such as exists at the rear of 10 Ω cm PERL cells), the above discussion of condition B→D (and beyond D) is still applicable for a cell in the dark. Hence, depending on the degree of inversion at equilibrium, the saturation behavior caused by this electrostatic effect may just be observed at low bulk injection levels in the dark; however, under illumination the surface will be under much stronger inversion and no saturation behavior will be observed (except possibly at extremely low light intensities).

For the accumulated case (such as exists at the n-diffused front surfaces of PERL cells) no saturation behavior can be caused by the electrostatic conditions at the oxide, since the recombination is always limited by the minority carriers at the Si/SiO_2 interface. An exception to this statement applies to the case of very light surface doping, only slight accumulation, and a large difference in σ_p and σ_n (with $\sigma_p>\sigma_n$ for the n-type case). Such a scenario exhibits essentially the same behavior as the flatband case below. The oxide structures at the front and rear of PERF cells are identical to the front oxide of the PERL cells, except that the rear n-type diffusion is often lighter and the rear oxide is covered with Al. Since the Al is annealed after deposition, both of these factors may result in a slightly lower D_{it} (and possibly Q_f); however, in all these cases the Si is accumulated and thus the electrostatic effect is not evident, unless the n diffusion is very light.

C. Flatband conditions

In a recent publication[7] we have shown that unequal capture cross sections alone can produce saturation behavior under flatband conditions. Indeed, in that work it was shown that for flatbands, recombination rate saturation only occurred if the electron and hole capture rates were unequal; however, the shape of the Si energy bands approaching the Si/SiO_2 interface is very rarely flat in practice (due to the combined effects of oxide charge, dopant depletion, and work-function differences), unless the "flatband" gate voltage is applied. For this reason, any asymmetry in the capture cross sections will, in general, only have the effect of enhancing or reducing the voltage range over which saturation occurs as described above.

D. Effect of saturation on S_{eff}

As can be seen from the results in Sec. IV, the behavior of n_s and p_s is rather different than that of n_b and p_b. Hence, because S_{eff} relates the surface recombination rate to the bulk excess minority-carrier concentration, it is not constant with increasing bulk injection. While simple analytical expressions can be obtained for some injection levels (as given in Sec. V A), for injection levels higher than those at saturation numerical calculations are required. The injection dependence of S_{eff} for p-type Si has been examined previously by Aberle and co-workers[18] and Otaredian[19] for the case of $\sigma_p<\sigma_n$, and spatially uniform doping. Here (Fig. 6), we calculate the injection dependence of S_{eff} for the case of equal capture cross sections with Q_f, d_{ox}, ϕ_m, and the dopant profile as measured at the rear of 1 Ω cm PERL cells (with $V_G=0$). The form of the curve is very similar to those obtained by Aberle and co-workers, Otaredian, and from other experimental measurements on oxidized p-type Si.[48–51]

E. Lateral ohmic voltage drop within inversion layers

Shoulders have been observed[2] in the dark $I-V$ curves of PERF cells (with an n-type diffusion at the rear). As mentioned above, the n-diffused Si adjacent to the oxides in PERF cells is accumulated, so no saturation caused by the electrostatic effects described above can occur in these regions. It is possible, though, that some electrons are transported through the n-type layer to recombine at the oxidized

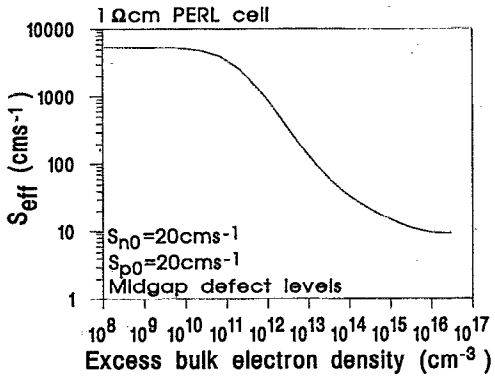

FIG. 6. S_{eff} at the rear surface of a 1 Ω cm PERL cell calculated as a function of bulk injection level, for interface states at midgap with equal electron and hole capture cross sections (see Table II for cell parameters).

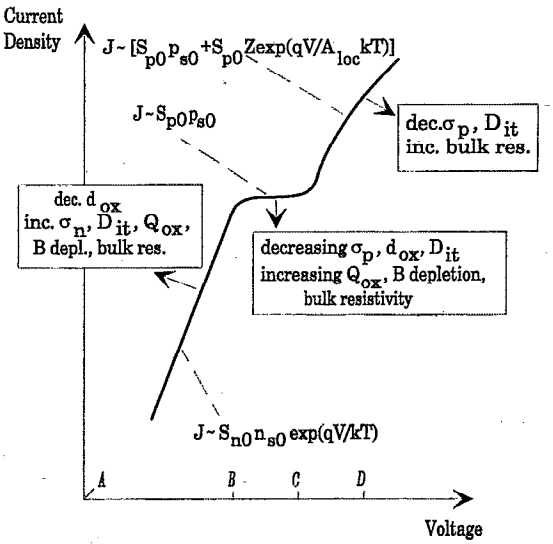

FIG. 7. Schematic representation of a typical surface recombination current caused by the electrostatics at a Si–SiO_2 interface as a function of device voltage. Also shown are arrows indicating the directions each line segment would move if the MOS parameters were changed as indicated. Z is a prefactor whose magnitude changes with the local ideality factor.

p-type surface regions around the point contacts. In this scenario the n-type layer would facilitate the electrostatic saturation effect occurring in these (small area) p-type regions; however, a preliminary 2D investigation of PERF cells performed using DESSIS$_{ISE}$ shows that this is not capable of dominating the behavior of the existing PERF cells. Alternatively, if the p-type surface regions have been significantly degraded (by more than a factor of 10 relative to the PERL rear surfaces), these regions may not require lateral conduction through the n layer in order to dominate the dark $I-V$ curve; however, no evidence is presently available which would suggest that the p-type surface regions of the PERF structures are any more heavily defected than those in the PERL cells.

It has been suggested[2] that in PERF cells an ohmic voltage drop builds up across a shunt conductance from the n-type layer to the rear contact or in the rear n-type layer itself, as the device voltage is increased. A shunt conductance could arise from a pinhole through the oxide or direct shunting of, or tunneling through, the rear p^+-n junction (formed between the uncontacted n layer and the heavily diffused p-type region near the rear point contacts). This controls the lateral transport of electrons through the n-layer toward points of high recombination, and produces a saturation of the recombination rate in these regions when the ohmic voltage drop increases sufficiently. Our preliminary 2D investigation of PERF cells confirms this behavior, suggesting that pinholes are most probably the cause for the saturation effects observed in the $I-V$ curves of these cells. A more detailed discussion of the behavior of PERF cells is beyond the scope of this article, and the reader is referred to Ref. 2.

As is evident from the preceding sections, the combined effects of oxide charge, Al coverage, and boron depletion produce inversion conditions at the rear surface of (p-type) PERL cells for some forward-bias voltages. Under these conditions the PERL and PERF structures are quite similar, and one might therefore expect saturation resulting from lateral conduction effects (particularly those due to pinholes in the rear oxide) to occur in PERL cells. The 2D simulations of PERL cells outlined in Sec. IV, and further simulations which included the effects of pinholes, suggest that this is indeed the case. However, its magnitude is negligible in comparison to other recombination mechanisms in the cells (in particular, the rear Si/SiO_2 interface recombination described above), so that this phenomenon has no influence on the dark or illuminated $I-V$ curves of PERL cells.

The lateral current in the PERL inversion layers is very small due to their limited conductivity (even for 10 Ω cm substrates). There is some evidence that boron diffusions significantly degrade the lifetime in the diffused and surrounding material.[54] Consequently, simulations have also been performed with reduced effective lifetimes (much smaller than those previously estimated from experimental measurements) in the contact and base regions, but carriers then flow directly to the rear contact regions and the lateral conduction effect is again negligible.

VI. CONSISTENCY WITH EXPERIMENTAL MEASUREMENTS

A. Recombination currents

In the foregoing discussion the emphasis has been on the recombination rates at Si/SiO_2 interfaces, with some discussion of lateral transport of electrons along the rear surface of PERL (and PERF) cells to points of high recombination. This recombination behavior manifests itself as recombination currents which can be measured directly, if they dominate the cell's dark or J_{sc}-shifted illuminated $I-V$ characteristics.[7]

A schematic representation of a typical rear-surface recombination current in a p-type Si solar cell which exhibits the electrostatic saturation behavior is shown in Fig. 7. The low-voltage section of the $I-V$ curve has unity ideality factor since the recombination is electron limited and $n_s \sim \exp(qV/kT)$ (condition A→B in PERL cells). Saturation of the recombination rate produces a shoulder in the curve at medium device voltages, where the recombination rate is

hole limited and the hole concentration increases only very slowly with V (condition B→C). As the surface approaches strong inversion and beyond, the recombination rate remains hole limited, but the functional dependence of p_s on V is rather complex (Sec. IV). However, to a good approximation $\Delta p_s \sim \exp(qV/AkT)$ with "local ideality factor" A varying between 1 and 2 (condition C→D). As previously mentioned, if the degree of band bending or the ratio σ_p/σ_n is large, the saturation region may be reduced, or even missing; however, due to the change in A factor, one still observes a shoulder in the $I-V$ characteristics. In real devices, the $I-V$ curve is the sum of contributions from all regions within the device. Thus, in practice the high-bias ($1<A<2$) current is often "overtaken" by a recombination current with smaller ideality factor, arising from some other mechanism (such as base recombination).

The variation of basic shape of the recombination current in Fig. 7 with σ_p, σ_n, Q_f, d_{ox}, bulk resistivity, and the degree of dopant depletion is also indicated in the figure. It should be noted that for high S_{n0} values (larger than about 50 cm s^{-1} for 1 Ω cm PERL cells), essentially every electron reaching the rear Si/SiO_2 interface recombines, over the section of the curve below the shoulder. The rate-limiting process is then the transport of the electrons to the interface rather than the electron (or hole) capture at the interface.[14] Hence, increasing S_{n0} (or equivalently σ_n or D_{it}) only shifts the low-voltage section of the curve in the direction shown in Fig. 7 until this "threshold" value is reached. The knowledge of the variation of the recombination current with MOS parameters can be used for future design/fabrication changes in order to achieve higher efficiency. In particular, when the recombination current represents the J_{sc}-shifted illuminated curve, it is important to shift the shoulder down while keeping the high-voltage section of the curve as low as possible (i.e., as far down and to the right-hand side as possible). The shoulder should then be below the maximum power point (MPP) and the fill factor improved.

Implicit in the discussions in Secs. IV and V was that the shoulder in the J_{sc}-shifted rear surface recombination current-voltage curve under illumination is displaced to lower current and voltage levels than applicable to the dark curve of the same cell. So, although the shape is as shown in Fig. 7 in both cases, the curves do not satisfy the principle of superposition.[3] Indeed, in the case of the 1 Ω cm PERL cells analyzed here, it is the curve labeled $p_s - p_s(V=0)$ in Fig. 4(b) which indicates the shape of the J_{sc}-shifted rear surface recombination current under 1 sun illumination (for an explanation of this statement, the reader is referred to Ref. 3). The shoulder is shifted down so far that it is no longer noticeable (within the resolution limits of the device simulator); however, the high local ideality factors for this curve mean that the total recombination current (which contains a large contribution from the base) still exhibits a slight shoulder which does affect the MPP and fill factor.

B. Measured PERL $I-V$ curves

In Fig. 8 we compare the measured dark and illuminated $I-V$ characteristics (taken at 25 °C) of a typical recent-generation 1 Ω cm PERL Si solar cell fabricated at UNSW

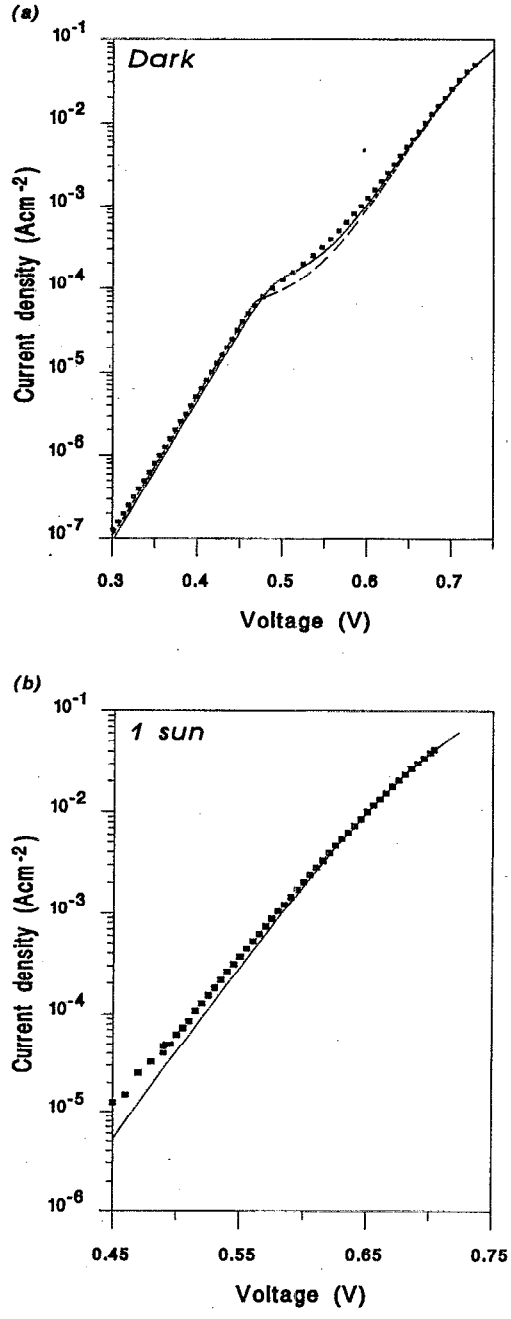

FIG. 8. Measured and calculated (a) dark and (b) illuminated $I-V$ characteristics of a typical 1 Ω cm PERL Si solar cell. The solid squares are the measured data while the lines are obtained from 2D simulations. The dashed line in (a) corresponds to a 2D simulation with $S_{n0}=1000$ cm s^{-1} and $S_{p0}=10$ cm s^{-1} at the rear Si/SiO_2 interface, while the solid lines in both (a) and (b) are the simulated curves for $S_{n0}(\text{rear})=S_{p0}(\text{rear})=20$ cm s^{-1} (other parameters given in Table II). Both the measured and simulated illuminated curves have been shifted from the fourth to the first quadrant by their short-circuit currents.

with the results of the 2D simulations performed using DESSIS$_{ISE}$ (using the parameters of Tables I and II). Note that the illuminated $I-V$ curve has been shifted by its short-circuit current (from the fourth to the first quadrant) in order that it represents the recombination currents under illumination.[55] The simulation results have been corrected for the measured series resistance of the PERL cells[56] and the

calculated perimeter effect.[20] Excellent agreement is obtained using the measured oxide parameters (allowing for the uncertainty in each of the measured parameters).

The present version of DESSIS$_{ISE}$ only supports a single type of defect level at the Si/SiO_2 interface, so a varying σ_p/σ_n ratio as suggested by the work of Yablonovitch *et al.*[41] for simulation of the cell in the dark could not be included. According to Yablonovitch's *et al.* results σ_p/σ_n(rear)=0.01 (for the dominant interface states) for voltages up to condition B, so a dark $I-V$ curve was simulated with $S_{n0}=1000$ cm s^{-1} and $S_{p0}=10$ cm s^{-1} (which is shown as a dashed line in Fig. 8). For voltages greater than or of the order of those corresponding to condition B, n_s/p_s at the rear is such that interface states with near-equal cross sections would be expected to dominate. Therefore, a second dark $I-V$ curve has been simulated with equal capture cross sections for electrons and holes at the rear Si/SiO_2 interface ($S_{n0}=S_{p0}=20$ cm s^{-1}, shown as a solid line in Fig. 8). In Fig. 8(a) it can be seen that the measured data up to the shoulder is best fitted by the unequal capture cross sections while the shoulder section is best fitted by equal capture cross sections. Thus, the (high-current) envelope of these two $I-V$ curves provides the best complete fit to the experimental data. However, it should be noted that both simulations provide a good fit to the experimental data, so one cannot infer anything conclusive about the capture cross-section ratios for interface states from the $I-V$ measurements alone.

For the calculated surface electron and hole carrier concentrations under illumination, σ_p/σ_n at the rear Si/SiO_2 interface is predicted by Yablonovitch *et al.* to lie in the 1–80 range for all bias voltages. At the higher voltages where the J_{sc}-shifted illuminated $I-V$ data is more reliable, the σ_p/σ_n ratio is predicted to approach unity. Hence, the simulations under illumination were performed using exactly the same values for σ_p (rear) and σ_n (rear) as were used for the dark simulation with equal capture cross sections (i.e., $S_{n0}=S_{p0}=20$ cm s^{-1}). Above $V=600$ mV ($\sim V_{MPP}$), excellent agreement is evident, while the simulated illuminated $I-V$ curve diverges from the measured data at low voltages [see Fig. 8(b)]. The currents at such voltages in the illuminated curve are the difference between two large values (close to the short-circuit current) due to the shifting procedure. Hence, the separation of the simulated curve and measured data represents an error of only approximately 0.05%, and could easily be due to drift in light intensity during measurement, or a result of the extrapolation of the V_{oc} and V_{MPP} perimeter-effect calculations[20] to lower voltages.

A very close fit to PERL $I-V$ curves has previously been obtained using a less complete model (than that employed here) of the rear surface oxide.[6,7,20] This earlier work already predicted that the rear oxidized surface is responsible for the observed shoulders in the $I-V$ curves. Analysis of the magnitude of the recombination currents at the interfaces using the new DESSIS$_{ISE}$ model confirmed that the low-medium-voltage section of the dark $I-V$ curve is indeed dominated by recombination at the rear Si/SiO_2 interface. Similarly, although under 1 sun illumination the rear-surface recombination has already been saturated at short circuit by the photogenerated carriers, it still contributes significantly to the recombination at MPP, in agreement with the earlier model. At higher bias voltages (both in the dark and under illumination) the recombination within the bulk regions of the base is also significant (as previously predicted[20]), resulting in lower local ideality factors than would occur if the rear surface remained dominant. Further, under the AM1.5 spectrum, the front surface recombination becomes important.[20]

Our old model also accurately determined the extent to which the efficiency of the cell is affected by the rear surface saturation effect, but the details of the mechanism were partly obscured by the approximations made of the rear MOS structure. In particular, we assumed that the effect of the Al coverage could be approximated by extra oxide charge, in a bare oxide structure. As noted in Sec. II, for thick oxides (as are used at the rear of PERL cells) the Al/p-Si work-function difference can be relatively closely approximated; however, the partial balancing of (the real) Q_f by Q_m is not properly included by such an approximation. Furthermore, the boron depletion effect was not considered at all in the above work.

The question may well be asked: Why have the surface recombination saturation effects discussed here not been observed in many other high-efficiency Si solar cells? Clearly, the remainder of the cell must be of sufficiently high quality that the oxide recombination dominates. Second, depletion or weak inversion conditions must exist in the Si at the oxide, and one must examine the device behavior over a sufficiently large bias voltage range, to observe the shoulder. Similar shoulders in dark $I-V$ curves have been reported by Beier and Voss,[57] King, Gee, and Hansen,[58] and Neugroschel and Mazer,[59] and these may well be caused by the mechanisms described here. However, several other mechanisms can also result in such shoulders (such as bulk or depletion region recombination saturation, ohmic limitation of lateral conduction in surface channels, or grain-boundary recombination), so it is crucial to measure as many cell parameters as possible independently, in order to distinguish between the possible causes.

VII. CONCLUSION

It has been shown that the behavior of the electrons and holes under the electrostatic conditions at oxidized silicon surfaces can produce a saturation in the surface recombination rate, for surfaces depleted (or slightly inverted) at equilibrium. This produces a shoulder both in the semilogarithmic dark and J_{sc}-shifted illuminated $I-V$ curves, if this recombination is dominant in the device. Unequal electron and hole capture cross sections can either accentuate or reduce this effect, except for flatband conditions where a σ_p/σ_n ratio less than unity (for oxidized p-type Si) is required.

The clear result of this work is that the electrostatic conditions at the rear oxidized surface of high-efficiency PERL Si solar cells fabricated at UNSW are responsible for the observed saturation behavior in their dark and illuminated $I-V$ curves. Furthermore, the improved understanding of the precise mechanism of surface recombination outlined in this work suggests the following options for design/fabrication improvements: A very light rear n-type diffusion, an increased positive oxide charge, a decreased oxide thickness,

and/or an increase in the boron depletion would act to shift the shoulder in the J_{sc}-shifted illuminated $I-V$ curve to lower currents (below MPP). These processing changes should not cause an increase in either D_{it} or σ_p, if the changes are to be effective. The difficulty here is that there is no generally accepted microscopic picture of the relationship between these MOS parameters and the properties of the interface states (such as D_{it} or σ_p). There is, however, some evidence that high oxide charge is linked to high-interface-state densities. A further practical hurdle in the case of decreasing oxide thickness is the observed higher probability of pinholes in the oxide resulting from imperfections introduced during the oxide formation.

ACKNOWLEDGMENTS

The authors acknowledge contributions of other members of the Centre for Photovoltaic Devices and Systems to this work, in particular J. Zhao, A. Wang, and X. Dai who processed the PERL and PERF cells, Y. H. Tang for help with the SUPREM calculations, and A. B. Sproul and A. W. Stephens for their comments on the theory. The determination of oxide parameters was performed by S. Glunz from Fraunhofer-Institute ISE, Germany, SR profiles by Solecon Laboratories in California, USA, and SIMS measurements were made by K. Prince at the Australian Nuclear Science and Technology Organization in Sydney, Australia. We also thank U. Krumbein from ETH-Zurich for his help with the simulations. S.J.R. gratefully acknowledges the financial support of an Australian Postgraduate Research Award and P.P.A. the support of a fellowship of the Foundation for Handicapped Academics, Liechtenstein. This work was supported by the Australian Research Council and the Energy Research and Development Corporation. The Centre for Photovoltaic Devices and Systems is supported by the Australian Research Council's Special Research Centres Scheme and Pacific Power.

APPENDIX: INTERFACE TRAPPED CHARGE

The statistics of charge trapped in interface states satisfy the following equation:[16]

$$Q_{it} = -q\int_{E_V}^{E_C} D_{it,A}(E) f_A(E)\,dE + q\int_{E_V}^{E_C} D_{it,D}(E) f_D(E)\,dE, \tag{A1}$$

where $f_A(E)$ is the electron-occupancy function of acceptor states, and $f_D(E)$ the hole occupancy of donor states, which are given by

$$f_A(E) = \frac{\sigma_{n,A} n_s + \sigma_{p,A} p_1}{\sigma_{n,A}(n_s + n_1) + \sigma_{p,A}(p_s + p_1)} \tag{A2}$$

and

$$f_D(E) = \frac{\sigma_{n,D} n_1 + \sigma_{p,D} p_s}{\sigma_{n,D}(n_s + n_1) + \sigma_{p,D}(p_s + p_1)}, \tag{A3}$$

with n_1 and p_1 as defined in Eq. (17). Note that the capture cross sections, n_1 and p_1 are all energy dependent, and that $f_A(E) = [1 - f_D(E)]$ if the capture cross sections for donor and acceptor states are identical.

A number of difficulties are encountered when attempting to apply the above equations to an arbitrary grown oxide. For interface-state energies close to the band edges $\{n_1$ or $p_1\} \gg \{n_s, p_s\}$ independent of the injection level (for the injection levels of interest here). Examining the behavior of Eqs. (A2) and (A3), one can see that the occupancy of the states near the band edges essentially does not change with injection. Thus, in $C-V$ measurements such as those used for this work, the measured value of Q_f contains this injection-independent Q_{it}. Although the total $D_{it}(E)$ has been measured (including for PERL cells), the proportions of acceptor and donor states (as functions of energy) have never been clearly established. Furthermore, as mentioned in Sec. III, only either the electron or hole capture cross section has in general been measured for a particular state.

However, in PERL cells, the maximum change in Q_{it} with injection is at least an order of magnitude smaller than the measured fixed charge Q_f for the following reasons. The measured D_{it} (including both acceptors and donors) near midgap is less than 5×10^9 cm^{-2} eV^{-1} (see Table I). Also, since the states near the band edges (which have a higher D_{it}) do not significantly change their occupancy over the injection levels of interest, the range of energies of interface states whose occupancy does change is only about half the band gap (i.e., about 0.6 eV). Thus, the maximum possible change in Q_{it} with injection is of the order of 3×10^9 cm^{-2}. In contrast, the measured value of Q_f is greater than 5×10^{10} cm^{-2} (which, as mentioned, may include a contribution from the injection-independent Q_{it}).

Hence, in the case of the oxides found in PERL cells (and other similar oxides) the explicit Q_{it} statistics need not be included, since their effect is relatively small. A qualitative understanding of the effect of trapped charge can thus be obtained once one knows the general behavior of the interface carrier concentrations (and then checked for consistency by considering small changes to an "effective Q_f" value). As is shown in Sec. IV, for p-type Si and a positive Q_f, the interface electron concentration increases with bulk injection while the hole concentration remains approximately constant, until strong inversion conditions are approached at the surface. Beyond this point both carrier concentrations increase, but at a slower rate and $n_s > p_s$. Examining the behavior of Eq. (A2) under these conditions, one finds that f_A is approximately constant, or increases, with increasing injection. Similarly, from Eq. (A3) f_D decreases with increasing injection. Therefore, $(Q_f + Q_{it})$ reduces slightly, since Q_{it} becomes more negative. Note that this has the effect of reducing the degree of band bending relative to that without the trapped charge (for a given injection level), which in turn reduces the interface electron concentration slightly, further reducing the effect of Q_{it}. This is very similar to the Fermi-level pinning which is observed at grain boundaries[60] and Schottky barriers.[61]

[1] A. Wang, J. Zhao, and M. A. Green, Appl. Phys. Lett. **57**, 602 (1990).
[2] S. R. Wenham, S. J. Robinson, X. Dai, J. Zhao, Y. H. Tang, A. Wang, A. Ebong, C. B. Honsberg, and M. A. Green, in Proceedings of the 1st World Conference on Photovoltaic Energy Conversion (WCPEC), Waikoloa Hawaii, December 5–9, 1994.
[3] S. J. Robinson, A. G. Aberle, and M. A. Green, J. Appl. Phys. **76**, 7920 (1994).
[4] M. A. Green, S. R. Wenham, J. Zhao, A. Wang, X. Dai, A. Milne, M. Taouk, J. Shi, F. Yun, B. Chan, A. B. Sproul, and A. W. Stephens, Final Report Sandia Contract No. 66-5863, Sandia National Laboratories, Albuquerque, March 1992.
[5] A. G. Aberle, S. J. Robinson, A. Wang, J. Zhao, S. R. Wenham, and M. A. Green, Prog. Photovoltaics **1**, 133 (1993).
[6] A. G. Aberle, G. Heiser, and M. A. Green, J. Appl. Phys. **75**, 5391 (1994).
[7] S. J. Robinson, A. G. Aberle, and M. A. Green, IEEE Trans. Electron Devices **ED-41**, 1556 (1994).
[8] D. R. Frankl, Surf. Sci. **3**, 101 (1965).
[9] A. S. Grove, and D. J. Fitzgerald, Solid-State Electron. **9**, 783 (1966).
[10] F. Hurkx, H. L. Peek, J. W. Slotboom, and R. A. Windgassen, IEEE Trans. Electron Devices **ED-40**, 2273 (1993).
[11] G. J. Rees, Solid-State Electron. **28**, 517 (1985).
[12] P. De Visschere, Solid-State Electron. **29**, 1161 (1986).
[13] M. W. Hillen and J. Holsbrink, Solid-State Electron. **26**, 453 (1983).
[14] S. R. Dhariwal and D. R. Mehrotra, Solid-State Electron. **31**, 1355 (1988).
[15] M. Y. Ghannam and R. P. Mertens, IEEE Trans. Electron Devices **ED-10**, 242 (1989).
[16] R. B. M. Girisch, R. P. Mertens, and R. F. De Keersmaecker, IEEE Trans. Electron Devices **ED-35**, 203 (1988).
[17] X. Correig, J. Calderer, E. Blasco, and R. Alcubilla, Solid-State Electron. **33**, 477 (1990).
[18] A. G. Aberle, S. Glunz, and W. Warta, J. Appl. Phys. **71**, 4422 (1992).
[19] T. Otaredian, Solid-State Electron. **36**, 905 (1993).
[20] A. G. Aberle, P. P. Altermatt, G. Heiser, S. J. Robinson, A. Wang, J. Zhao, U. Krumbein, and M. A. Green, J. Appl. Phys. **77**, 3491 (1995).
[21] E. H. Nicollian and J. R. Brews; *MOS (Metal Oxide Semiconductor) Physics and Technology* (Wiley, New York, 1982).
[22] S. M. Sze, *Physics of Semiconductor Devices*, 2nd ed. (Wiley, New York, 1981).
[23] M. A. Green and J. Shewchun, Solid-State Electron. **17**, 349 (1974).
[24] J. Zhao, A. Wang, P. P. Altermatt, S. R. Wenham, and M. A. Green, in Proceedings of the 1st World Conference on Photovoltaic Energy Conversion (WCPEC), Waikoloa Hawaii, December 5–9, 1994.
[25] A. G. Aberle, S. W. Glunz, A. W. Stephens, and M. A. Green, Prog. Photovoltaics **2**, 265 (1994).
[26] W. Füssel, R. Könenkamp, M. Schmidt, and H. Flietner, in *Proceedings of the 11th EC PV Solar Energy Conference*, Montreux, Switzerland (Harwood, Switzerland, 1992), p. 746.
[27] S. W. Glunz (private communication).
[28] K. E. Prince (private communication).
[29] H. F. Wolf, *Semiconductors* (Wiley, New York, 1971), Chap. 4.
[30] *VLSI Technology*, edited by S. M. Sze, 2nd ed. (McGraw-Hill, New York, 1988), p. 129.
[31] S. Margalit, A. Neugroschel, and A. Bar-Lev, IEEE Trans. Electron. Devices **ED-19**, 861 (1972).
[32] C. P. Ho, J. D. Plummer, S. E. Hansen, and R. W. Dutton, IEEE Trans. Electron Devices **ED-30**, 1438 (1983).
[33] P. A. Schumann, Jr. and E. E. Gardner, J. Electrochem. Soc. **116**, 87 (1969).
[34] Dickey and Ehrstein, N.B.S. Special Publication 400-48, May 1979.
[35] C. P. Wu, E. C. Douglas, and C. W. Mueller, IEEE Trans. Electron Devices **ED-22**, 319 (1975).
[36] E. H. Nicollian, M. H. Hanes, and J. R. Brews, IEEE Trans. Electron Devices **ED-20**, 380 (1973).
[37] G. E. McGuire, in *Deposition Technologies for Films and Coatings*, edited by R. F. Bunshah (Noyes, Park Ridge, NJ, 1982), pp. 548–568; L. C. Feldman and J. W. Meyer, *Fundamentals of Surface and Thin Analysis* (Elsevier, Amsterdam, 1986).
[38] R. R. King, R. A. Sinton, and R. M. Swanson, IEEE Trans. Electron Devices **ED-37**, 365 (1990).
[39] J. R. Davis, Jr., A. Rohatgi, R. H. Hopkins, P. D. Blais, P. Rai-Choudhury, J. R. McCormick, and H. C. Mollenkopf, IEEE Trans. Electron Devices **ED-27**, 677 (1980).
[40] D. P. Parton and T. Markvart, in *Proceedings of the 12th EC PV Solar Energy Conference and Exhibition*, Amsterdam, Netherlands (H. S. Stephens & ASSDC, Felmersham, UK, 1994), p. 508.
[41] E. Yablonovitch, R. M. Swanson, W. D. Eades, and B. R. Weinberger, Appl. Phys. Lett. **48**, 245 (1986).
[42] N. Stein and H. Röppischer, Phys. Status Solidi A **123**, 139 (1991).
[43] W. Warta (private communication).
[44] M. J. Uren, K. M. Brunson, and A. M. Hodge, Appl. Phys. Lett. **60**, 624 (1992).
[45] S. Müller, K. Kells, J. Litsios, U. Krumbein, A. Schenk, and W. Fichtner, SIMUL 1.2.1: *Manual* (Integrated Systems Laboratory, ETH, Zürich, 1992).
[46] W. Shockley and W. T. Read, Phys. Rev. **87**, 835 (1952); R. N. Hall, *ibid.* **87**, 387 (1952).
[47] M. A. Green, *High Efficiency Silicon Solar Cells* (Trans. Tech., Zürich, Switzerland, 1987).
[48] J. A. Eikelboom, C. Leguijt, and A. R. Burgers, in *Proceedings of the 12th E. C. Photovoltaic Solar Energy Conference and Exhibition*, Amsterdam, Netherlands (H. S. Stephens & ASSCD, Felmersham, UK, 1994), p. 1782.
[49] S. W. Glunz, A. B. Sproul, S. Sterk, and W. Warta, in *Proceedings of the 12th E. C. Photovoltaic Solar Energy Conference and Exhibition*, Amsterdam, Netherlands (H. S. Stephens & ASSDC, Felmersham, UK, 1994), p. 492.
[50] A. W. Stephens, A. G. Aberle, and M. A. Green, J. Appl. Phys. **76**, 363 (1994).
[51] R. R. King, R. A. Sinton, and R. M. Swanson, in *Conference Record, 19th IEEE Photovoltaic Specialists Conference*, New Orleans, LA (IEEE, New York, 1987), p. 1168.
[52] M. A. Green, A. W. Blakers, J. Zhao, A. Wang, A. M. Milne, X. Dai, and C. M. Chong, Report SAND89-7041, Sandia National Laboratories, Albuquerque, 1989.
[53] A. G. Aberle, W. Warta, J. Knobloch, and B. Voss, in *Conference Record, 21st IEEE Photovoltaics Specialists Conference*, Kissimmee, FL (IEEE, New York, 1990), p. 233.
[54] S. K. Ghandi, *VLSI Fabrication Principles* (Wiley, New York, 1983).
[55] F. A. Lindholm, J. G. Fossum, and E. L. Burgess, IEEE Trans. Electron Devices **ED-26**, 165 (1979).
[56] A. G. Aberle, S. R. Wenham, and M. A. Green, in *Conference Record, 23rd IEEE Photovoltaics Specialists Conference*, Louisville, KY (IEEE, New York, 1993), p. 133; P. P. Altermatt, G. Heiser, A. G. Aberle, S. J. Robinson, and M. A. Green (unpublished).
[57] J. Beier and B. Voss, in *Conference Record, 23rd IEEE Photovoltaics Specialists Conference*, Louisville, KY (IEEE, New York, 1993), p. 321.
[58] D. L. King, J. M. Gee, and B. R. Hansen, in *Conference Record, 20th IEEE Photovoltaics Specialists Conference*, Las Vegas, NV (IEEE, New York, 1988), p. 555.
[59] A. Neugroschel and J. A. Mazer, IEEE Trans. Electron Devices **ED-29**, 225 (1982).
[60] H. J. Queisser and J. H. Werner, in Proceedings of the Materials Research Society Symposium, 1988, Vol. 106, p. 53.
[61] J. Bardeen, Phys. Rev. **71**, 717 (1947).